

Alloying driven transition between ferro- and antiferromagnetism in UTGe compounds: the $\text{UCo}_{1-x}\text{Ir}_x\text{Ge}$ case

Dávid Hovančík^{1,2}, Akinari Koriki^{1,3}, Anežka Bendová¹, Petr Doležal¹, Petr Proschek¹, Martin Míšek⁴, Marian Reiffers², Jan Prokleška¹, Jiří Pospíšil¹ and Vladimír Sechovský¹

¹*Charles University, Faculty of Mathematics and Physics, Department of Condensed Matter Physics, Ke Karlovu 5, 121 16 Prague 2, Czech Republic*

²*University of Presov, Faculty of Humanities and Natural Sciences, 17 Novembra 1, 081 16 Presov, Slovakia*

³*Hokkaido University, Graduate School of Science, Department of Condensed Matter Physics, Kita10, Nishi 8, Kita-ku, Sapporo, 060-0810, Japan*

⁴*Institute of Physics, Academy of Sciences of Czech Republic, v.v.i, Na Slovance 2, 182 21 Prague 8, Czech Republic*

Abstract

The evolution of magnetic properties of isostructural and isoelectronic solid solutions of the superconducting itinerant $5f$ -electron ferromagnet UCoGe with antiferromagnet UIrGe was studied by magnetization and specific heat measurements of a series of $\text{UCo}_{1-x}\text{Ir}_x\text{Ge}$ compounds at various temperatures and magnetic fields. The ferromagnetism in UCoGe was found to have vanished already for the lowest studied Ir substitution for Co ($x = 0.005$) whereas superconductivity appears to persist up to $x = 0.01$. The antiferromagnetism of UIrGe is gradually suppressed with decreasing Ir concentration to disappear by $x \approx 0.75$. The section of the T - x phase diagram in the range $0.005 \leq x < 0.75$ is dominated by a paramagnetic phase. With increasing Ir concentration for $x > 0.4$, antiferromagnetic correlations gradually appear in a paramagnetic state, which may eventually lead to frozen incoherent spin configurations at low temperatures. These results are clearly in stark contrast to the behavior of the related $\text{URh}_{1-x}\text{Ir}_x\text{Ge}$ system, which exhibits a discontinuous transformation between the ferromagnetic and antiferromagnetic phases of parent compounds at a critical Rh-Ir concentration. The striking difference is due to the different degrees of the localization of U $5f$ -electron states in the weak itinerant ferromagnet UCoGe and the local moment ferromagnet URhGe .

*Corresponding author: Dávid Hovančík

E-mail: hovancikd@gmail.com

Keywords: UCoGe , UIrGe , URhGe , UTe_2 ferromagnetism, antiferromagnetism, paramagnetism, quantum critical point, phase diagram,

INTRODUCTION

Orthorhombic UTX (T - transition metal, X - a p -electron element) uranium compounds of TiNiSi-type structure are of constant interest due to the extraordinary richness of various magnetic and superconducting states and other strongly correlated electron phenomena. Special attention was paid to URhGe [1] and UCoGe [2] due to the unique coexistence of ferromagnetism (FM) and superconductivity (SC). The evolution of magnetism with increasing distance of U nearest neighbors within the series of UTGe compounds seems to follow Hill's scenario ADDIN EN.CITE [3-5] when starting by the paramagnetic (PM) ground state of URuGe followed up by ferromagnets UCoGe[2] and URhGe[1] and antiferromagnets (AFM) UIrGe ADDIN EN.CITE [6, 7], UNiGe ADDIN EN.CITE [8-10] and UPdGe ADDIN EN.CITE [11, 12]. Despite this empirical finding, the evolution of magnetism in pseudo-ternary alloy systems is often unexpectedly different. This confirms the fact that the microscopic origin of the magnetism in these compounds is more complex than determined only by the overlaps of the $5f$ -orbitals of the nearest-neighbor U ions. The strong role of competing FM and AFM interactions mediated by the $5f$ -ligand hybridization determining the magnetic ground state was predicted for these compounds ADDIN EN.CITE [13, 14] as well as for the recently discovered nonmagnetic heavy-fermion superconductor UTe₂ ADDIN EN.CITE [15, 16].

The superconducting phenomena in these materials seem to be related not only to their magnetic ground states but also to various paramagnetic modes, which develop at much higher temperatures. However, the nature of these relationships remains unexplained. The unusual features of the ferromagnetic and paramagnetic states in the uranium ferromagnetic superconductors have been revealed by studies of their pseudo-ternary alloy systems ADDIN EN.CITE [17-19]. UIrGe is isostructural and isoelectronic UCoGe and URhGe but on contrary, it exhibits an antiferromagnetic ground state and doesn't show superconductivity.

It is, of course, of natural interest to see the effect of alloying UIrGe with the two ferromagnetic superconductors. The URh_{1-x}Ir_xGe case has been studied and results published earlier[14]. The key feature of the system is the discontinuity at $x_{\text{crit}} = 0.56$ in all the magnetic parameters between the ferromagnetic and antiferromagnetic phase typical for the first-order transition.

These aspects motivated us to investigate also the UCo_{1-x}Ir_xGe system by measurements of magnetization and specific heat at various temperatures and magnetic fields. Results of our present study indicate that on contrary to the behavior of the URh_{1-x}Ir_xGe system, the UIr_{1-x}Co_xGe compounds have a paramagnetic ground state in a rather wide range of intermediate concentrations. The specific-heat and magnetization anomalies showing up at elevated temperatures can be understood as effects of strong AFM correlations and/or freezing of incoherent configuration of magnetic moments with possible short-range magnetic order.

EXPERIMENTAL

To study the development of the magnetic states in the UCo_{1-x}Ir_xGe system we have prepared a series of polycrystalline samples with different Co/Ir concentrations to fully cover all regions of expected interesting magnetic property changes. All samples were prepared by arc melting from the stoichiometric amounts of the elements (purity of Co 4N5, Ge 6N, and Ir 4N). U was purified by the solid-state electrotransport technique[27], following our previous experience with the preparation of UCoGe[27]. The arc-melting process was realized under a protective Ar (6N purity) atmosphere on a water-cooled Cu crucible. Each sample was three times turned upside down and subsequently re-melted to achieve the best homogeneity. All samples were separately wrapped into a Ta foil (99.99%), sealed in a quartz tube under a vacuum of $\sim 10^{-6}$ mbar, annealed at 900 °C for 7 days, and then slowly cooled down to room temperature to avoid the creation of internal stresses. Each sample was characterized by X-ray powder diffraction (XRPD) at room temperature on a Bruker D8 Advance diffractometer. The obtained data were evaluated by the Rietveld technique[28] using FULLPROF/WINPLOTR software[29,30], given the previously

published crystallographic data of the isostructural UCoGe [31] and UIrGe [24] compounds as starting models.

Two single crystals of compositions of $\text{UCo}_{0.6}\text{Ir}_{0.4}\text{Ge}$ and $\text{UCo}_{0.08}\text{Ir}_{0.92}\text{Ge}$ were grown by Czochralski pulling in a tri arc furnace using pulling speeds of 6 mm/h. The single crystals were several centimeters long cylinders with a diameter of 2-3 mm. The pulled crystals were wrapped in Ta foil, sealed in a quartz tube under the vacuum 10^{-6} mbar, and annealed for 14 days at 900°C . The quality of single crystals was verified by the Laue method and composition using the same analysis as polycrystalline samples. Oriented samples in the form of cubes for magnetization measurement were prepared using a fine abrasive wire saw.

The chemical composition was verified by a scanning electron microscope Tescan Mira I LMH equipped with an energy dispersive X-ray detector Bruker AXS. The specific heat (C_p) measurements were performed on thin polished plates using the relaxation method on a PPMS9T with a ^3He insert. Magnetization (M) data were obtained on powder samples wrapped into the plastic ampoules using the VSM option of the PPMS9T and PPMS14T devices and the extraction method in an MPMS 7T magnetometer.

RESULTS AND DISCUSSION

Lattice parameters

The XRPD analysis confirmed the orthorhombic TiNiSi -type structure (space group $Pnma$) of all samples over the entire concentration range in the $\text{UCo}_{1-x}\text{Ir}_x\text{Ge}$ series. All three lattice parameters show a linear dependence on x obeying Vegard's law see (Fig. 1)[20]. The increasing trend of the lattice param-

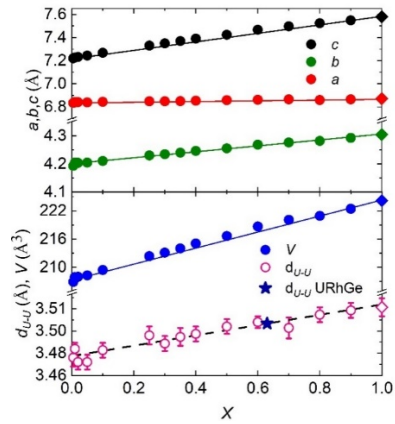


FIG. 1. The concentration dependence of the room temperature lattice parameters, unit cell volume, and d_{U-U} distance of the $\text{UCo}_{1-x}\text{Ir}_x\text{Ge}$ samples. The lines serve as guides to the eye.

ters reflects a considerable difference between the covalent radii of the Co (126 pm) and Ir (141 pm) atoms [21]. The dependence of the lattice parameters and the distance between nearest-neighbor U ions (d_{U-U}) on x is very similar to that of the $\text{UCo}_{1-x}\text{Rh}_x\text{Ge}$ [22] presumably because of an almost identical transition elements radii ($\text{Rh} \approx \text{Ir}$). Likewise, the value of the d_{U-U} distance in both cases crosses Hill's critical value ($d_{U-U} \approx 3.5 \text{ \AA}$) at the same position $x \sim 0.6$.

Magnetization

The low-field (0.01 T) thermomagnetic curves (Fig. 2) $x \leq 0.3$ (Fig. 2(a)) monotonously increase with decreasing temperature. For increasing $x \geq 0.3$ they gradually more saturate at low temperatures and for $x \geq 0.4$ the $M(T)$ curves show a maximum. A maximum on an $M(T)$ curve may be due to several reasons: a

magnetic phase transition to an AFM state, freezing of glassy spins configurations, short-range AFM ordering, or AFM correlations in a paramagnetic phase. For $x \leq 0.7$ the $M(T)$ curve has a more or less symmetric bump-shape whereas the anomaly for $x \geq 0.8$ terminates on the low-temperature side that is resembling the $M(T)$ curve exhibited by the UIrGe single crystal in fields applied along the b - [14] and c -axis [23], respectively.

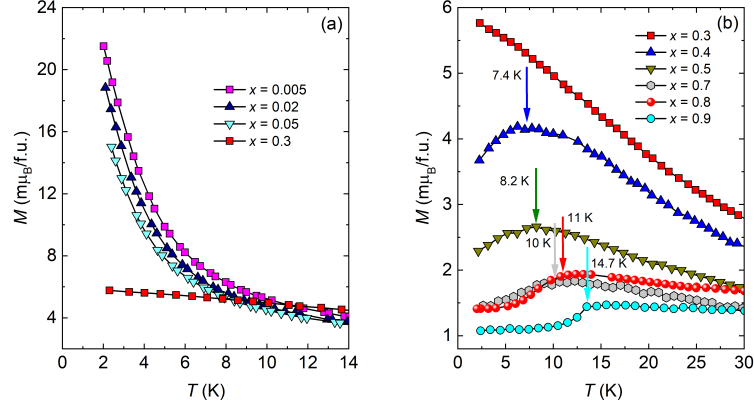


FIG. 2. (a) The thermomagnetic curves measured on selected $\text{UCo}_{1-x}\text{Ir}_x\text{Ge}$ samples in $H = 100$ mT for (a) $x \leq 0.3$ (b) $x \geq 0.3$. The vertical arrows indicate characteristic temperatures of $M(T)$ maximum.

Some of these features are naturally seen more clearly on the $M(T)$ curves measured on the $\text{UCo}_{0.6}\text{Ir}_{0.4}\text{Ge}$ and $\text{UCo}_{0.08}\text{Ir}_{0.92}\text{Ge}$ single-crystals (see Fig. 3), which were prepared for this purpose. The first crystal represents the compounds in the intermediate concentration range, which we assume paramagnetic down to the lowest measured temperatures. The single crystal enables us to see that the magnetization is strongly anisotropic. The easy-axis (c -axis) signal is about 5-times larger than the b -axis magnetization and the maximum of the c -axis magnetization appears at a considerably lower temperature than that of the b -axis magnetization. This indicates that this compound adopts the uniaxial anisotropy characteristic for UCoGe. On the other hand, the $\text{UCo}_{0.08}\text{Ir}_{0.92}\text{Ge}$ crystal exhibits magnetization behavior qualitatively similar to UIrGe, reflecting antiferromagnetism with an XY-type anisotropy. The transition to the AFM state at T_N for both field directions can be associated with a sharp drop on the low-temperature side of the anomaly.

The measurement of the $\text{UCo}_{0.08}\text{Ir}_{0.92}\text{Ge}$ single crystal has also shown that the maximum of the b -axis magnetic susceptibility at the temperature $T_{\text{max},b}$ ($= 18$ K) is higher than T_N ($= 14.6$ K). This feature reflecting strong magnetic correlations in a paramagnetic range at temperatures well above the magnetic ordering transition is observed in numerous heavy-fermion materials [24] and also in UCoGe and UIrGe. The value of $T_{\text{max},b}$ is much closer to T_N in $\text{UCo}_{0.08}\text{Ir}_{0.92}\text{Ge}$ than in UIrGe ($T_{\text{max},b} = 29$ K, $T_N = 16.5$ K) [18]. In this context, it is worth noting that the b - and c -axis magnetization (Fig. 3(a)) of $\text{UCo}_{0.6}\text{Ir}_{0.4}\text{Ge}$ single-crystal exhibit the maximum at very different temperatures ($T_{\text{max},b} = 29$ K, $T_{\text{max},c} = 7$ K).

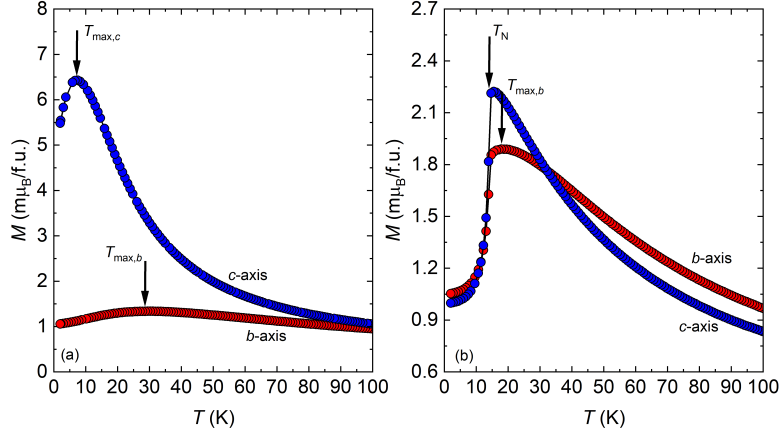


FIG. 3. The thermomagnetic curves measured on the single-crystals (a) $UC_{0.6}Ir_{0.4}Ge$ and (b) $UC_{0.08}Ir_{0.92}Ge$ in a magnetic field of 100 mT applied parallel to the c and b -axis, respectively.

The low-field concave curvature of the 2-K magnetization isotherms (Fig. 4) measured for $x \leq 0.15$ signals the proximity of ferromagnetism and the isotherms gradually straighten with increasing Ir content up to $x = 0.5$. The isotherm for $x = 0.6$ is almost straight. A closer inspection reveals a slight smooth S-shape character which signifies a stronger involvement of antiferromagnetic interactions. The $M(B)$ curve for $x = 0.7$ is qualitatively similar to that for $x = 0.6$, only the slope is considerably lower. The isotherms for $x \geq 0.8$ show a sudden increase of slope at a certain field followed by an almost linear increase.

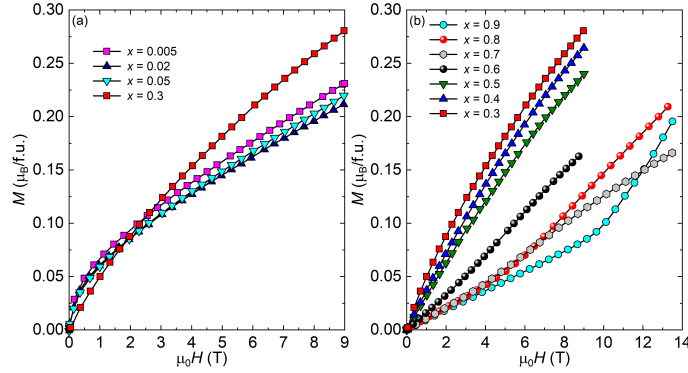


FIG. 4. The 2-K magnetization isotherms of selected $UC_{0.1-x}Ir_xGe$ samples for (a) $x \leq 0.3$ and (b) $x \geq 0.4$.

The 2-K magnetization isotherms measured on the $UC_{0.6}Ir_{0.4}Ge$ single crystal (Fig. 5(a)) are rather characteristic for a strongly anisotropic paramagnet although the thermomagnetic curves (Fig. 3) show a maximum characteristic for considerable involvement of antiferromagnetic correlations. The c -axis magnetization at 2K is much stronger than the b -axis signal. The corresponding field dependences are qualitatively different. The c -axis magnetization shows a strong saturation tendency whereas the b -axis data show a linear dependence.

The c -axis 2-K isotherm of the $UC_{0.08}Ir_{0.92}Ge$ crystal (Fig. 5(b)) exhibits a large double step jump at ≈ 12.5 T, which reflects a metamagnetic transition at this critical field H_c , similar to $UIrGe$. Considering the $T_N/\mu_0 H_c$ ratio obtained for $UIrGe$, the 2-K metamagnetic transition may be expected at $\mu_0 H_c \sim 12$ T and 18 T in $H \parallel c$, $H \parallel b$, respectively for $UC_{0.08}Ir_{0.92}Ge$. This assumption has been corroborated by the aforementioned result in the c -axis field whereas the b -axis magnetization isotherm is linear up to the maximum field of the measurement. The measurements in b -axis fields higher than 18T are desired to confirm our prediction.

The two-step nature of the transition may qualitatively resemble the behavior of another UTGe compound, specifically UNiGe [9], which exhibits well-distinguished two-step metamagnetic transitions in the b -axis and c -axis magnetic field. The closeness of the two steps in our case leads to a suspicion that the features could be understood to be due to signals of two mutually misoriented crystal grains. Such a possibility may also explain the appearance of the magnetization step between 11 and 12 T in b -axis data. A detailed metallographic analysis of the crystal and future experiments performed with magnetic fields even higher than the currently available 14 T may help to solve this uncertainty.

On the contrary, for the $\text{UCo}_{0.6}\text{Ir}_{0.4}\text{Ge}$ single-crystal no signs of a metamagnetic transition in the $M(H)$ dependence neither for the c - nor the b -axis are observed (Fig. 5(a)) corroborating the scenario that the interval $0.4 \leq x \leq 0.7$ can not be conceived in terms of an ordinary antiferromagnetic state.

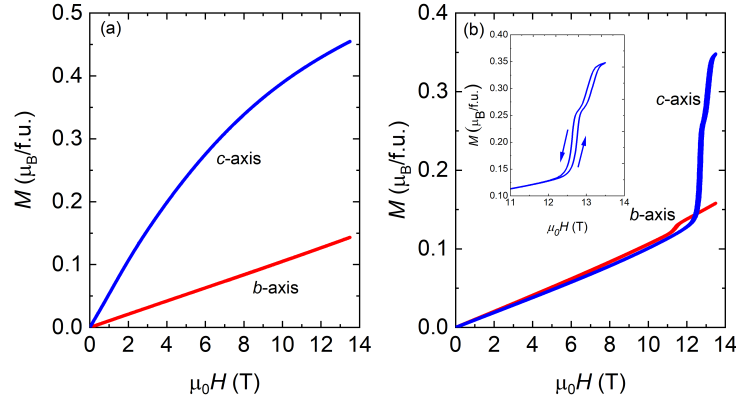


FIG. 5. The 2-K magnetization isotherms measured on (a) $\text{UCo}_{0.6}\text{Ir}_{0.4}\text{Ge}$ and (b) $\text{UCo}_{0.08}\text{Ir}_{0.92}\text{Ge}$ single crystals in magnetic fields applied parallel to the c - and b -axis, respectively. The inset shows the metamagnetic transition with tiny hysteresis in detail.

Specific heat

The specific heat data measured for all available polycrystalline samples are shown in Fig. 6. The T_C -related anomaly and the steep increase below 1 K associated with the onset of superconductivity in the C_P/T vs. T data measured on UCoGe are wiped out already from data measured on the sample with $x = 0.005$. The convex C_P/T vs. T curves for $x \geq 0.05$ gradually straighten with increasing x up to 0.4 where a broad bump appears on an almost straight C_P/T vs. T dependence. The bump develops gradually with further increasing Ir content. The bump growth suddenly accelerates when increasing x from 0.7 to 0.8. For $x = 0.9$ we observe a λ peak qualitatively similar to the T_N -related anomaly observed for UIrGe .

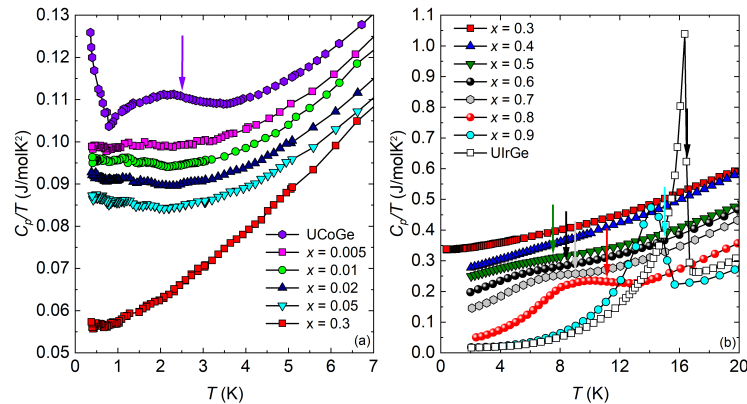


FIG. 6. The temperature dependences of specific heat (C_P/T vs T plots) in zero external magnetic field of $\text{UCo}_{1-x}\text{Ir}_x\text{Ge}$ compounds for (a) $x \geq 0.3$, for (b) $x \geq 0.3$. The arrows mark the characteristic temperatures for the construction of the T - x phase diagram. For the sake of clarity, the curves are shifted up by an increasing offset with decreasing x (for $x = 0.9$ and $x = 0.3$ (a) the data are original). Data for UCoGe are taken from Ref. ADDIN EN.CITE [19] and for UIrGe from[23].

To determine the magnetic entropy S_{mag} we have subtracted the phonon C_{ph} and electron C_{el} contribution from the experimental C_P data as shown in Fig. 7(a). Since the simple Debye $\sim T^2$ dependence does not provide a usable fit a general polynomial function with the dominant quadratic term was used. Fig. 7(a) shows a representative example. It is seen in Fig. 7(b) that S_{mag} dramatically decreases with decreasing x from $0.22 R \ln 2$ for $x = 1.0$ down to $\sim 0.07 R \ln 2$ for $x = 0.8$, which most likely reflects rapid suppression of the magnetic order with Co substitution for Ir. The further decrease of $S_{\text{mag}}(x)$ is then very slow with decreasing x from 0.7 to 0.4 and S_{mag} vanishes around 0.3.

The overall evolution of S_{mag} with decreasing Ir content is in line with the evolution of magnetization and specific-heat anomalies may be tentatively understood in terms of suppression of long-range AFM order at a critical concentration x_c between 0.8 and 0.7. The tiny broad bumps in C_P/T vs T observed for $0.3 < x \leq 0.7$ may be understood in terms of short-range AFM ordering, freezing of a glassy configuration of spins, or AFM correlations in the PM state similar to e.g. the CeRu_2Si_2 case[25].

The large difference between S_{mag} of UCoGe and UIrGe in conjunction with a qualitatively similar difference of U magnetic moments in the two compounds highlights the fact that the $5f$ -electron states in UCoGe are considerably more delocalized than in UIrGe .

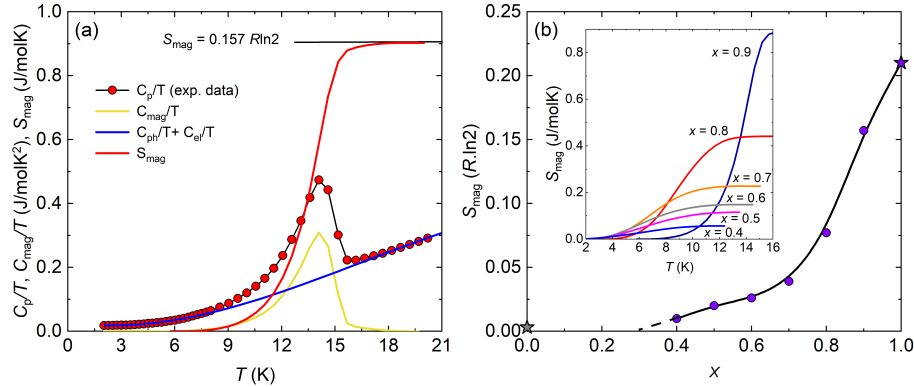


FIG. 7. (a) Temperature dependence of specific heat and its components (C_P/T vs T plots) and magnetic entropy S_{mag} for $x = 0.9$ and (b) the value of S_{mag} as a function of x expressed in the unit of $R \ln 2$. The inset shows S_{mag} versus T for AFM compounds. The value of S_{mag} for UCoGe and UIrGe (marked by the stars) were taken from Ref. ADDIN EN.CITE [26, 27].

Magnetic phase diagram

The magnetization and specific-heat data presented above allow us to sketch a tentative T - x magnetic-phase diagram for the $\text{UCo}_{1-x}\text{Ir}_x\text{Ge}$ system shown in Fig. 8. Information on the parent UCoGe and UIrGe compounds have been taken from the relevant literature sources [35, 22]. Already tiny Ir doping ($x = 0.005$) kills the weak itinerant FM of UCoGe while the superconductivity persists up to $x = 0.01$.

On the other hand, the AFM ordering in UIrGe survives at least up to the substitution of 20% Co for Ir in UIrGe . T_N steeply decreases with decreasing x from 1 to 0.8. The original rapid fall of T_N abruptly changes near between $x = 0.8$ and 0.7. In the concentration range $0.7 \geq x \geq 0.4$ the characteristic

temperatures of broad bumps in the M vs T and C_p/T vs T dependences decrease much slower with decreasing x (Figs. 6 and 8). One cannot entirely exclude the possibility of specific antiferromagnetic phases in this concentration range of the $\text{UCo}_{1-x}\text{Ir}_x\text{Ge}$ system similar to those proposed in the case of the $\text{UCo}_{1-x}\text{Pd}_x\text{Ge}$ compounds [28]. Rather, however, we tend to assume that the highest substitution disorder (see also [35]) in the intermediate concentration range causes the distribution of exchange interactions that lead to complex magnetic correlations in the paramagnetic state (correlated paramagnet – (CPM)) and ultimately to the freezing of incoherent spin arrangements (spin-glass-like, cluster glass [29] with possible short-range magnetic order (SRMO)). These phenomena lead to responses of the system like these we have observed in the concentration range $0.7 \geq x \geq 0.4$. One should be aware that this situation is caused also by a mixture of two T-metals with $3d$ and $5d$ valence electrons of significantly different bandwidths and different strength of spin-orbit interaction. The magnetism in $\text{UCo}_{1-x}\text{Ir}_x\text{Ge}$ compounds is further complicated by the strong and complex magnetocrystalline anisotropy that alters with various alloying of the mother compounds.

To prove the validity of our scenario, more work on single crystals should be done. The investigation should be extended to transport properties measurements, as well as to experiments that can address the microscopic aspects of magnetism in $\text{UCo}_{1-x}\text{Ir}_x\text{Ge}$ compounds more directly (magnetic neutron and X-ray scattering, in particular).

The paramagnetic state on the Co-rich side ($0.005 < x < 0.3$) was confirmed both by missing anomalies in specific heat data measured down to 0.4 K as well as in the temperature dependence of magnetic susceptibility. The initial Ir doping in UCoGe leads to the abrupt loss of ferromagnetism, and the paramagnetic state between $0.005 \leq x \leq 0.3$ is different than that in the interval $0.4 \leq x \leq 0.7$. Regardless of the missing ferromagnetic order, the electrical resistivity has shown traces of superconductivity for composition $x = 0.005$ and 0.01 just at the edge of the T - x phase diagram, which is similar behavior to the other $\text{UCo}_{1-x}\text{T}_x\text{Ge}$ systems [30].

The resulting T - x phase diagram of the $\text{UCo}_{1-x}\text{Ir}_x\text{Ge}$ system in Fig. 8 with a wide paramagnetic concentration region has completely different character in comparison to the magnetic phase diagram of $\text{URh}_{1-x}\text{Ir}_x\text{Ge}$ [14], which is characteristic by the discontinuity in all the magnetic parameters between the ferromagnetic and antiferromagnetic phase at $x_{\text{crit}} = 0.56$ typical for a first-order transition.

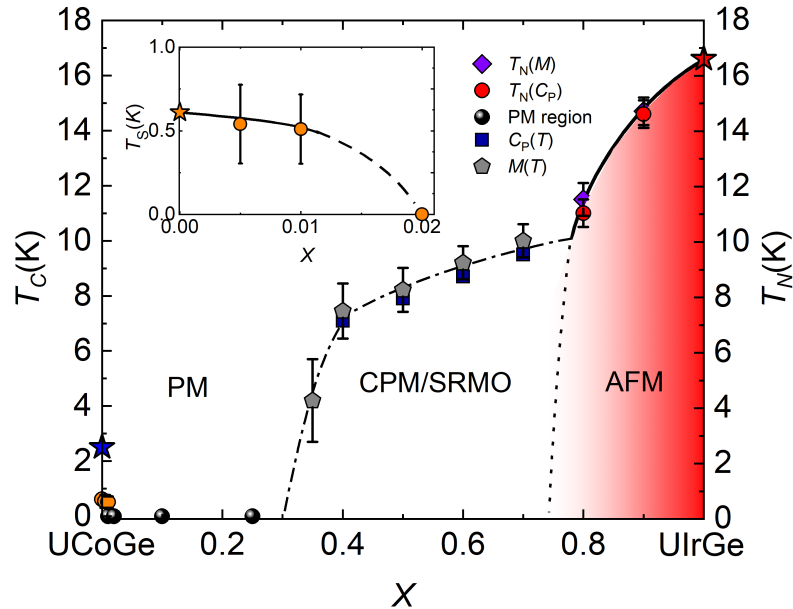


FIG. 8. T - x magnetic phase diagram of $\text{UCo}_{1-x}\text{Ir}_x\text{Ge}$ system. The inset shows the concentration dependence of temperature T_s of the onset of superconductivity determined from the electrical resistivity. The data for UCoGe and UIrGe (marked by stars) are taken from Refs.[31] and[32], respectively.

CONCLUSIONS

This work intended to explore the evolution of magnetism in the pseudo-ternary compounds of composition between the superconducting itinerant $5f$ -electron ferromagnet UCoGe and isostructural and isoelectronic antiferromagnet UIrGe . For this purpose, we have prepared a series of polycrystalline samples of UCoGe doped with Ir in the wide range of concentrations $\text{UCo}_{1-x}\text{Ir}_x\text{Ge}$ ($0.005 \leq x \leq 0.9$) and two representative single crystals ($\text{UCo}_{0.6}\text{Ir}_{0.4}\text{Ge}$, $\text{UCo}_{0.08}\text{Ir}_{0.92}\text{Ge}$) and studied them by measuring magnetization and specific heat at various temperatures and magnetic fields. The rich data set enabled us to construct the complex T - x phase diagram of the entire pseudo-ternary system.

The already very low doping of UCoGe by Ir ($x = 0.005$) leads to the instant suppression of ferromagnetism. Also, the superconductivity of UCoGe is suppressed rapidly by Ir doping. Nevertheless, traces of superconductivity were detected in the $x = 0.005$ and 0.01 samples.

Further increase of the Ir content reinforces the magnetic correlations resulting in a strange state in the interval $0.3 \leq x \leq 0.7$. In our view, we ascribe magnetic behavior in this concentration range to the paramagnetic state with strong FM/AFM correlations (a correlated paramagnet – (CPM)) and/or to the freezing of incoherent spin arrangements (spin-glass-like, cluster glass [29] with possible short-range magnetic order (SRMO)). Ordinary antiferromagnetism has been detected in the interval $0.8 \leq x \leq 1$ with an abrupt increase of T_N towards the parent UIrGe . The character of correlations depends on the evolution of U magnetic moments and the hierarchy of FM and AFM exchange interactions mediated by $5f$ -ligand hybridization $5f-3d/5d$ (U-Co / Ir), which is controlled by the composition of the Co/Ir sublattice.

Our present work in comparison with [14] experimentally demonstrates the fundamentally different transformation between the ferromagnetic and antiferromagnetic states of parent compounds in $\text{URh}_{1-x}\text{Ir}_x\text{Ge}$ and $\text{UCo}_{1-x}\text{Ir}_x\text{Ge}$ system, respectively. The striking difference is most probably due to the considerably different degree of the localization of U $5f$ -electron states in the weak itinerant ferromagnet UCoGe and the local moment ferromagnet URhGe .

The polycrystalline study has revealed basic knowledge about the T - x phase diagram of the $\text{UCo}_{1-x}\text{Ir}_x\text{Ge}$ system, but similarly, as in the neighboring alloy systems, a more complete single-crystal study is highly desirable to understand the system in detail. The evolution of the fundamentally important magneto-crystalline anisotropy throughout the system remained mostly uncovered. Nonetheless, the results obtained on the two available single crystals indicated its significant development throughout the system.

The paramagnetic phase regions in the $\text{UCo}_{1-x}\text{Ir}_x\text{Ge}$ system require further special attention because both parent compounds are characterized by the presence of the CPM regions existing above the different magnetic states and therefore the correlations can be of various natures. The rigorous investigation and understanding of the competition between the ferromagnetic and antiferromagnetic correlations is a substantial task in the $\text{UCo}_{1-x}\text{Ir}_x\text{Ge}$ system particularly in the frame of the detected CPM region in the recently discovered heavy-fermion superconductor UTe_2 .

Acknowledgments

The experiments were performed at MGML (<http://mgml.eu>), which is supported within the program of Czech Research Infrastructures (project no. LM2018096). This project was supported by OP VVV project MATFUN under Grant No.CZ.02.1.01/0.0/0.0/15_003/0000487. This project was supported by OP VVV project MATFUN under Grant No. CZ.02.1.01/0.0/0.0/15_003/0000487. The authors are indebted to Dr. Ross Colman for critical reading and correcting the manuscript.

REFERENCES

- ADDIN EN.REFLIST [1] D. Aoki, et al., *Nature* **413**, 613 (2001).
[2] N. T. Huy, et al., *Physical Review Letters* **99**, 067006 (2007).
[3] D. Aoki, et al., *Journal of the Physical Society of Japan* **81**, 011003 (2012).
[4] M. Vališka, et al., *Physical Review B* **92**, 045114 (2015).
[5] J. Pospíšil, et al., *Journal of the Physical Society of Japan* **86**, 044709 (2017).
[6] J. Pospíšil, et al., *Physical Review B* **98**, 014430 (2018).
[7] S. Yoshii, et al., *Journal of Physics: Conference Series* **51**, 151 (2006).
[8] S. Kawamata, et al., *Journal of Magnetism and Magnetic Materials* **104-107**, 51 (1992).
[9] F. R. de Boer, et al., *Physica B* **201**, 251 (1994).
[10] V. Sechovsky, et al., *Journal of Alloys and Compounds* **213-214**, 536 (1994).
[11] V. H. Tran, et al., *Journal of Magnetism and Magnetic Materials* **87**, 291 (1990).
[12] R. Troř, et al., *Journal of Magnetism and Magnetic Materials* **73**, 389 (1988).
[13] W. Knafo, et al., *Physical Review B* **100**, 094421 (2019).
[14] J. Pospíšil, et al., *Physical Review B* **95**, 155138 (2017).
[15] C. Duan, et al., *Physical Review Letters* **125**, 237003 (2020).
[16] S. Sundar, et al., *Physical Review B* **100**, 140502 (2019).
[17] N. T. Huy, et al., *Solid State Communications* **149**, 703 (2009).
[18] J. Pospíšil, et al., *Physical Review B* **98**, 014430 (2018).
[19] J. Pospíšil, et al., *Journal of the Physical Society of Japan* **80**, 084709 (2011).
[20] L. Vegard, *Zeitschrift für Physik* **5**, 17 (1921).
[21] B. Cordero, et al., *Dalton Transactions*, 2832 (2008).
[22] J. Pospíšil, et al., *Physical Review B* **102**, 024442 (2020).
[23] V. Sechovský, et al., *Physica B: Condensed Matter* **359-361**, 1126 (2005).
[24] D. Aoki, et al., *Comptes Rendus Physique* **14**, 53 (2013).
[25] M. J. Besnus, et al., *Solid State Communications* **55**, 779 (1985).
[26] K. Prokeř, et al., *Physical Review B* **60**, 9532 (1999).
[27] A. Gasparini, et al., *Physical Review B* **82**, 052502 (2010).
[28] D. Gralak, et al., *Journal of Solid State Chemistry* **242**, 175 (2016).
[29] S. Pakhira, et al., *Journal of Physics: Condensed Matter* **33**, 115802 (2020).
[30] J. Pospíšil, et al., *Journal of Applied Physics* **105**, 07E114 (2009).
[31] A. Gasparini, et al., *Journal of Low Temperature Physics* **161**, 134 (2010).
[32] A. Ramirez, et al., *Journal of Applied Physics* **61**, 3189 (1987).